



LAWRENCE  
LIVERMORE  
NATIONAL  
LABORATORY

# FY10 Report on EBS Evaluations, Level 4 Milestone (M4): M4508042504

M. Sutton, M. A. Serrano de Caro, J. A. Blink, W.  
G. Halsey

August 26, 2010

## **Disclaimer**

---

This document was prepared as an account of work sponsored by an agency of the United States government. Neither the United States government nor Lawrence Livermore National Security, LLC, nor any of their employees makes any warranty, expressed or implied, or assumes any legal liability or responsibility for the accuracy, completeness, or usefulness of any information, apparatus, product, or process disclosed, or represents that its use would not infringe privately owned rights. Reference herein to any specific commercial product, process, or service by trade name, trademark, manufacturer, or otherwise does not necessarily constitute or imply its endorsement, recommendation, or favoring by the United States government or Lawrence Livermore National Security, LLC. The views and opinions of authors expressed herein do not necessarily state or reflect those of the United States government or Lawrence Livermore National Security, LLC, and shall not be used for advertising or product endorsement purposes.

This work performed under the auspices of the U.S. Department of Energy by Lawrence Livermore National Laboratory under Contract DE-AC52-07NA27344.

# Used Fuel Disposition Campaign

## Disposal Systems Evaluations and Tool Development – Engineered Barrier System Evaluation (Work Package LL1015080425)

### *FY10 Report on EBS Evaluations Level 4 Milestone (M4): M4508042504*

Lawrence Livermore National Laboratory

Mark Sutton, James A. Blink, William G. Halsey and  
Magdalena A. Serrano de Caro

#### **The Disposal Systems Evaluation Framework**

As part of the Disposal Systems Evaluations and Tool Development - Engineered Barrier System (EBS) Evaluation of the Used Fuel Disposition (UFD) Campaign within the Fuel Cycle Technology Office of DOE-NE, waste disposal of a range of potential waste forms is being considered in a range of geologic environments.

For each waste form and geologic environment combination, there are multiple options for a repository conceptual design. The Disposal Systems Evaluation Framework (DSEF) is being developed to formalize the development and documentation of options for each waste form and environment combination.

The DSEF is being implemented in two parts. One part is a *Microsoft Excel* workbook with multiple sheets. This workbook is designed to be user friendly, such that anyone within the UFD campaign can use it as a guide to develop repository conceptual designs that respect thermal, geometric, and other constraints. The other part is a *Microsoft Access* relational database file that will be centrally maintained to document the ensemble of conceptual designs developed with individual implementations of the Excel workbook.

The DSEF Excel workbook includes sheets for waste form, environment, geometric constraints, engineered barrier system (EBS) design, thermal, performance assessment (PA), materials, cost, and fuel cycle system impacts. Each of these sheets will guide the user through the process of developing internally consistent design options, and documenting the thought process. The sheets will interact with each other to transfer information and

identify inconsistencies to the user. In some cases, the sheets will be stand-alone, and in other cases (such as PA), the sheets will refer the user to another tool, with the user being responsible to transfer summary results into the DSEF sheet. Finally, the DSEF includes three top-level sheets: inputs & results, interface parameters, and knowledge management (i.e. references to reports, models, and publications such as the degradation mode surveys discussed below). These sheets will enable the user to see the overall picture on only a few summary sheets, but develop the design option systematically using the detailed sheets.

The DSEF Access relational database file will collect the key inputs, results, and interface parameters from each Excel workbook implementation. The power of a relational database will then be available to sort and organize groups of designs, and to answer queries about what evaluations have been done in the UFD campaign.

As an initial step in identifying candidate engineered-materials for this range of waste forms and environments, LLNL is reviewing the material science literature. A logical place to start is the degradation mode surveys historically performed for the unsaturated tuff environment of Yucca Mountain.

### **Review of Degradation Mode Surveys**

These degradation mode surveys were documented [e.g. Farmer, 1988a/b, Gdowski, 1988a/b and Bullen, 1988] for waste package candidate materials to be used at Yucca Mountain, including three austenitic alloys (304L, 316L and Alloy 825) and three copper alloys (CDA 102, CDA 613 and CDA 715) used in the nuclear industry and marine environments, respectively. The work contains information on phase stability, environmental effects of a repository, general corrosion, localized corrosion, stress corrosion cracking, hydride cracking, microbially-influenced corrosion and internal corrosion of candidate high-level radioactive waste (HLRW) package materials. Key features described in the degradation mode surveys are summarized below.

Elevated chromium, copper and nickel in steels typically yield superior corrosion resistance. The formation of a 1 – 5 nm Cr<sub>2</sub>O<sub>3</sub> layer on the surface of candidate austenitic alloys provides good protection from general corrosion and oxidation.

Environment / Alloy	304	316	825	CDA102	CDA613	CDA715
Atmospheric/Marine	<0.15	<0.01	<0.15	<1	<1	<1
Aqueous/Seawater	25			30	5	11
Hot Water (50, 80, 100°C)	<0.3	<0.3	<0.3			
Steam (100, 150°C)	<0.1	<0.1	<0.1			
Superheated Steam (566, 631°C)	7					
Water vapor (95°C) with gamma irradiation				4	2	6

Table 1. Approximate general corrosion rates,  $\mu\text{m}/\text{y}$  [Gdowski, 1988a].

Gamma irradiation of liquid films on candidate waste package material produces several oxidizing and reducing species by radiolysis that may increase intergranular stress corrosion cracking (IGSCC) in some sensitized alloys. It is assumed that nuclear waste package contents will not generate significant neutron flux.

Radiolysis of moist air and surface films causes hydrogen generation. Hydrogen has the potential to alter the metallurgical behavior of the container material, and it is important to examine the hydrogen diffusivity and solubility in such materials. For example, hydrogen solubility in 304 stainless steel (SS) ranges from  $\sim 100 - 300$  appm (at  $25 - 275^\circ\text{C}$ ). Low concentrations of hydrogen ( $\sim 30$  appm) have been shown to degrade primarily the ductility of the material hence making alloys more brittle.

Hydrogen embrittlement (HE) susceptibility appears to be related to the austenite-to-martensite transformation, with martensite being more susceptible to HE. No consensus is reported on the HE mechanism in austenitic steels. Furthermore, Gdowski [Gdowski, 1988b] states that there is a definite lack of literature on the effects of hydrogen in Alloy 825. Alloys with low carbon content ( $<0.03\%$  such as 304L, 316L and  $<0.05\%$  such as Alloy 825) have enhanced resistance to sensitization (which may translate into higher HE resistance) versus their higher carbon equivalent alloys (e.g. 304 and 316). However, literature suggests [Gdowski 1988b] HE *does* occur in 304L, 316L and Alloy 825. More recent Yucca Mountain-related work on HE will be reviewed in a subsequent UFD-EBS milestone.

Pitting resistance is typically higher in Alloy 825 than 304 or 316 steels, largely due to the increased Mo content in the alloy. Localized corrosion decreases with larger molybdenum additions.

The presence of certain microbial colonies on the surface of the waste package can lead to pitting corrosion. Reducing bacteria form hydrogen compounds (such as hydrogen sulfide), while oxidizing bacteria can in some cases oxidize elements of steel (such as iron), causing rust. Microenvironments can persist between the microbial colony and the material surface, preventing repassivation, concentrating pH effects, or accelerating hydrogen corrosion effects. MIC has been observed in 304L and 316L, but no catastrophic MIC was observed in Alloy 825.

Stress corrosion cracking (SCC) appears under a very specific combination of conditions, namely material susceptibility, tensile stress and aggressive environment. SCC of 304L and 316L U-bend samples has been observed in high chloride environments at elevated temperature. Resistance to SCC is largely due to higher nickel additions.

Welds can also affect the properties and behavior of the materials. For austenitic steels, problems include weld-induced sensitization, hot cracking, sigma-phase formation, and corrosion of the weld filler metal. Of concern are resistance to corrosion, hot cracking and formation of intermetallic phases. Heat affected zones (HAZ) of welds can be affected by the precipitation of  $\text{Cr}_{23}\text{C}_6$ . Both 304L and 316L have low carbon content, minimizing the formation of the carbide, while 825 contains titanium which preferentially forms carbides. When the compositions of 304L and 316L are adjusted to include 5% ferrite structure, impurities in the alloy are attracted to the ferrite and segregated from the grain boundary, thus preventing grain boundary cracking. Additionally, during the welding of 304L and 316L, a brittle sigma-phase can form. In Alloy 825, ferrite inclusion is not possible, so Alloy 625 is used as a weld-filler. The use of a different material for weld-filler can lead to the formation of a duplex microstructure containing both austenite (gamma-phase) and ferrite (alpha-phase). Literature on weld cracking of Alloy 825 is very limited.

During heat treatments such as welding (550 – 800°C), Cr-rich carbides precipitate along grain boundaries, causing Cr-depletion in the surrounding area to a level below the 13 – 15% required for passivation. Lower temperature sensitization (LTS, ~400°C) observed over longer periods of time could also be problematic, possibly for 304L and 316L, although high-nickel alloys may not be subject to LTS. However, there was no experimental evidence of a reduction in corrosion resistance due to LTS at the time of the degradation mode surveys of Farmer, et al [Farmer, 1988a].

After the degradation mode surveys were completed, the Yucca Mountain Program favored more corrosion-resistant alloys (i.e. progressing from Alloy 825 to 625 and then to Alloy 22, C-22). A literature search of Ni-Cr-Mo alloy degradation has been performed. The results are currently being reviewed and will be reported in a subsequent UFD-EBS milestone.

Additionally, a review of phase stability in Ni-Cr-Mo alloys, particularly relating to modeling using Calphad methodology [Turchi 2006] showed evidence of fcc matrix, long range order (LRO, Pt<sub>2</sub>Mo-type) formation of the oP6 phase, Frank-Kasper phases (P and  $\sigma$ ), carbides and silicides. The work also showed that the low Cr content excluded the formation of the sigma phase in alloy C-4. Similarly, the low Cr and Mo content in alloy C-276 significantly reduced the formation of the sigma phase and prevented the formation of the oP6 phase.

Understanding the kinetics of phase transformations is also important. Experimental work [Torres, 2003] provides evidence of phase transformations in Alloy 22, and concludes that in reality such phase transformations occur at a slower rate than predicted. The work by Turchi [Turchi, 2007] suggests that the Ni<sub>2</sub>Cr-type LRO transformation in Alloy 22 is slow enough such that it is not a concern for repository conditions (<200°C for 100,000 years).

The above material summarizes a lengthier summary of these references; that summary is included as appendices A through C. Work continues on library literature searches for the period between the degradation mode survey work by Farmer et al [Farmer, 1988a/b and Gdowski, 1988a/b] and present, as well as a review of the international literature for the range of geologic environments that have been investigated. Full references are given in the appendix sections, following.

*Appendix A* includes reviews of the degradation mode surveys plus additional information regarding phase transformation and kinetics.

*Appendix B* contains definitions of waste characteristics and waste environment.

*Appendix C* contains mechanical properties of several austenitic steels at room temperature.

## **Appendix A**

One task of the Yucca Mountain Site Characterization Project (YMP) was to select a material from which to fabricate high-level radioactive-waste (HLRW) containers for the potential repository. In this appendix, we briefly summarize the results of a survey study performed in 1988 [Farmer, 1988a] for candidate materials considered for the conceptual design (CD) of the HLRW containers of the YMP Site Characterization Plan (SCP).

In 1988 the review was conducted on YMP SCP degradation due to

- General Corrosion of Waste Packages
- Microbially Influenced Corrosion (MIC) of Waste Packages
- Stress Corrosion Cracking (SCC) of Waste Packages
- Localized Corrosion of Waste Packages
- Corrosion in Welds
- Hydride Cracking of Waste Packages
- Internal Corrosion of Waste Packages Prior to Breach

All these degradation mechanisms except microbiological corrosion were included in the survey study.

### **Waste Repository Requirements**

Containers must maintain mechanical integrity for 50 years, and complete containment of the waste for 300 to 1000 years. Heat generation leads to container peak temperature of ~250°C, decaying to 150°C after 100 years.

### **Candidate Materials**

Three austenitic alloys (304 L, 316 L and Alloy 825) and three copper alloys (CDA 102, CDA613 and CDA715) were selected in the 1988 survey [Farmer, 1988a], see Table A1a and Table A1b, respectively. The 3 austenitic alloys are used in the nuclear industry. The three copper alloys are used in marine environments.

Table A1a: Chemical composition of austenitic candidate alloys.

Element	304L	316L	Alloy 825
C	0.03 max	0.03 max	0.05 max
Mn	2.00 max	2.00 max	1.0 max
Si	1.00 max	1.00 max	0.5 max
Cr	18.0–20.0	16.0–18.0	19.5–23.5
Ni	8.0–12.0	10.0–14.0	38.0–46.0
P	0.045 max	0.045 max	—
S	0.03 max	0.03 max	0.03 max
Cu	—	—	1.5–3.0
Ti	—	—	0.6–1.2
N	0.10	0.10	—
Mo	—	2.0–3.0	3.0
Fe	Bal.	Bal.	Bal.

Table A1b: Chemical composition of Cu-based candidate alloys.

Alloy	Cu	Ni	Al	Mn	Sn	Fe	Zn	Other
CDA 102	99.95	—	—	—	—	—	<0.001	Pb < 0.001 Cd < 0.001 S < 0.0018 Hg < 0.0001 P < 0.003
CDA 613	90.82	0.05	6.75	0.16	0.20	2.46	0.01	Pb < 0.01 Co < 0.01
CDA 715	69.18	29.60	—	0.51	—	0.53	0.07	Pb, 0.01 P, 0.002 C, 0.04 S, 0.01

Note the presence of high Cr content in the austenitic candidate alloys. At least 12% (w/w) Cr is necessary for the formation of a protective Cr-oxide film. Control of the C content reduces the precipitation of Cr-rich  $M_{23}C_6$  carbides at the grain boundary (GB), namely the “sensitization” of the material. Addition of Ti eliminates this problem in Alloy 825. In other words, the addition of Ti stabilizes Alloy 825 against sensitization (see next section). Also, note the addition of Mo in 316L SS and Alloy 825 for pitting resistance in aqueous corrosion applications. The presence of Cu in Alloy 825 grants resistance to sulfuric acid.

## Oxidation and Corrosion

General corrosion and oxidation is reviewed in [Gdowski, 1988a]. The authors conclude that the formation of thin uniform Cr-oxide ( $Cr_2O_7$ ) layers (10-50 Å thick) on the surface provides the exceptional resistance of the candidate austenitic alloys to general corrosion and oxidation.

- Atmospheric corrosion rates of 304 (similar to 304L) and Alloy 825 in marine atmospheres are low (below  $\sim 0.15 \mu\text{m}/\text{y}$ ) with 316 (similar to 316L) ranked as the best material with atmospheric corrosion rate in marine atmosphere below  $\sim 0.01 \mu\text{m}/\text{y}$ .
- Aqueous corrosion rate of 304 in seawater (Panama Canal) is large ( $\sim 25 \mu\text{m}/\text{y}$ ),  $\sim 7 \mu\text{m}/\text{y}$  in superheated steam (566 and 621°C); this might limit the container lifetime in such environments.
- The austenitic candidate alloys will be resistant to general corrosion and oxidation in hot water and steam. Aqueous corrosion rates of 304L, 316L and Alloy 825 are all below  $\sim 0.3 \mu\text{m}/\text{y}$  in hot water (50, 80, 100°C) and below  $\sim 0.1 \mu\text{m}/\text{y}$  in steam (100 and 150°C).

Similar analysis is performed [Gdowski, 1988a] for Cu-based alloys. CDA 613 shows the best corrosion resistance to general corrosion and oxidation. The authors note that atmospheric and aqueous corrosion are the least significant modes of degradation; i.e. other corrosion mechanisms are expected to be life limiting (see next section).

- Atmospheric corrosion rates of CDA 102, CDA 613 and CDA 715 in marine atmosphere are below  $\sim 1 \mu\text{m}/\text{y}$
- Aqueous corrosion rates of CDA 102 and CDA 715 in seawater immersion are large ( $\sim 30 \mu\text{m}/\text{y}$  and  $\sim 11 \mu\text{m}/\text{y}$ ). CDA 613 is the best (corrosion rate  $\sim 5 \mu\text{m}/\text{y}$ ).
- General corrosion rates of CDA 102 and CDA 715 under gamma irradiation in air nearly saturated with water vapor (moist air) at 95°C are large ( $\sim 4$  and  $6 \mu\text{m}/\text{y}$ , respectively). Again CDA 613 is the best (corrosion rate  $\sim 2 \mu\text{m}/\text{y}$ ).

## **Environmental Effects in the Repository**

Nuclear waste containers will be exposed to high gamma radiation. It is assumed that the container surface might be covered by a thin liquid (water) layer, which is irradiated by  $\gamma$ -photons from the decay of radionuclides in the waste. Section 7 of the degradation mode survey [Farmer, 1988b Vol.3] gives a summary on the effect of  $\gamma$  radiation on stress corrosion cracking of sensitized 304 SS and Alloy 825. In general,  $\gamma$  irradiation of aqueous solutions produces several oxidizing and reducing species by radiolysis. Irradiation of liquid water by  $\gamma$  rays produces, ionic, free radicals and molecular products that are very chemically reactive, i.e. radical products ( $\text{H}^+$ ,  $\text{OH}^-$ ,  $e^-_{\text{aq}}$ ,  $\text{HO}_2$ ) and molecular products  $\text{H}_2\text{O}_2$ ,

and H<sub>2</sub>. The literature survey shows that  $\gamma$  radiation increases the intergranular stress corrosion cracking (IGSCC) susceptibility of sensitized 304 SS in high temperature oxygenated pure water. Experiments performed by Furuya et al. [Furuya, 1985] in boiling deionized water (100°C) show that  $\gamma$  irradiation ( $\gamma$  flux  $\sim 1.1 \times 10^7$  R/h) promotes IGSCC in sensitized 304 SS, see Fig. A1. He also reports that Alloy 825 exhibited no SCC with or without  $\gamma$  irradiation. From the work of Furuya et al. [Furuya, 1985] we conclude that Alloy 825 shows no change in its resistance to SCC in the presence of  $\gamma$  irradiation. Note that the conclusions are still open for 304 SS since the literature survey shows contradictory results for sensitized 304 SS; i.e. other authors found a beneficial effect of  $\gamma$  irradiation on 304 SS.

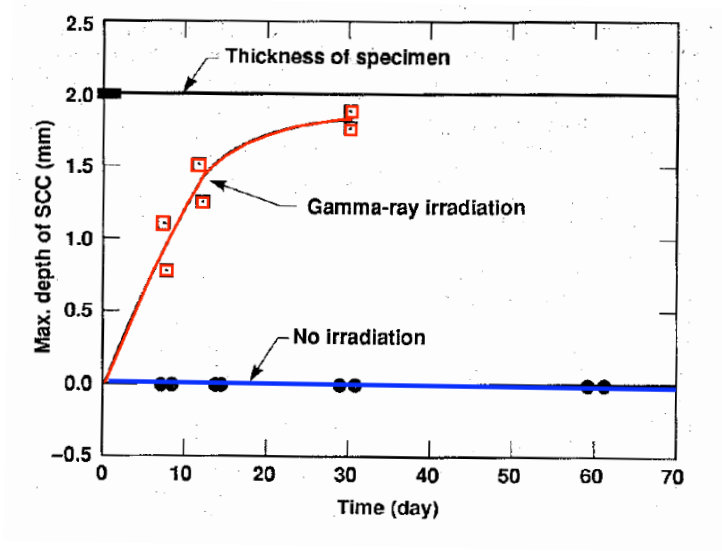


Figure A1:  $\gamma$  irradiation promotes an increase in the IGSCC susceptibility of sensitized 304 SS [Furuya, 1985]

The effect of fast ( $E > 1$  MeV) neutron irradiation followed by high gamma irradiation on SCC of 304 SS has been studied by several authors but is not reported here since it is assumed that nuclear-waste containers will not be subjected to significant neutron flux.

### Biological Corrosion (MIC) of Candidate Materials

Biological corrosion cannot be ruled out, even in the unfavorable environment near the waste package that includes high temperature, high  $\gamma$ -dose, and dryness. The bacteria

*Gallionella* and *Sphaerotilis* most commonly cause MIC in SS. MIC has been found in 304L and 316L SS [Pope, 1987]; especially on welds. No catastrophic MIC has been reported for Alloy 825.

## Stress Corrosion Cracking (SCC)

SCC is a type of localized corrosion characterized by fine cracks, which can propagate quite rapidly leading to failure of the component and potentially the associated structure. SCC appears under a very specific combination of three conditions:

1. The use of materials that are susceptible to SCC
2. Tensile stress, either from structural loading or present as residual stresses from forming or welding operations during manufacture and installation; and
3. The presence of a specific aggressive environment.

These conditions were met for 304L (9% Ni, w/w) and 316L (12% Ni, w/w) U-bend specimens immersed in 0.8% NaCl and HCl (pH 2.2) at 141°C where SCC was observed after 30 days exposure [Asphahani, 1975]. No SCC was observed in Alloy 825 with higher Ni content (43%, w/w). Higher resistance to SCC is linked to higher Ni content as shown in Fig. A2 where several Fe-Cr-Ni wires were exposed to a boiling 42% MgCl<sub>2</sub> solution. Alloys with more than 45-50% Ni (w/w) showed higher resistance to chloride cracking.

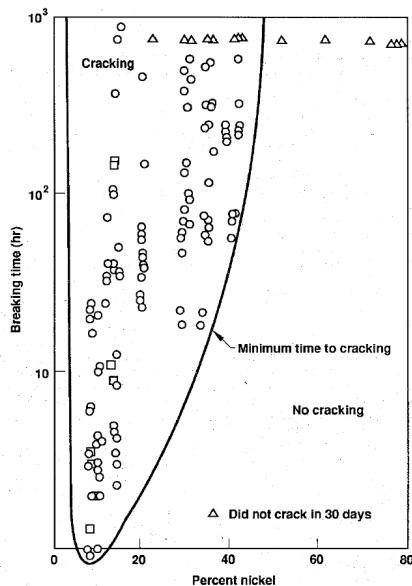


Figure A2: Susceptibility to SCC is higher for alloys with low Ni content [Copson, 1959].

As discussed in [Gdowski, 1991], the high Ni and Mo contents in Alloy C-276 (and other alloys such as Alloy G) is suggested as the reason for its exceptional resistance to SCC in acidic NaCl, and in boiling 42% MgCl<sub>2</sub> solutions.

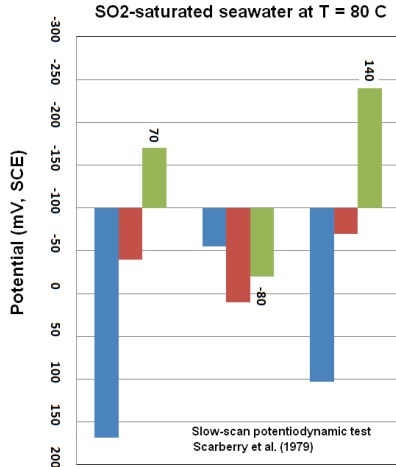
### Pitting Resistance

Resistance to pitting is quantified as the difference  $E_c - E_{corr}$ , where  $E_c$  is the pitting potential and  $E_{corr}$  is the corrosion potential. The more positive the difference  $E_c - E_{corr}$  is, the more resistant the alloy is to pitting. Pitting of 304, 316 SS and Alloy 825 was studied in two different substitute ocean water environments at  $T = 80^\circ\text{C}$ : 1) deaerated and 2) SO<sub>2</sub>-saturated, using immersion tests, slow-scan (0.6 V/h) and fast scan (50 V/h) potentiodynamic techniques [Scarberry et al, 1979]. These experiments show that Alloy 825 is the most resistant to pitting, see as an example Table A2 and Fig. A3 with results obtained using the slow-scan technique for the pitting potential,  $E_c$ , corrosion potential,  $E_{corr}$ , and resistance to pitting defined as  $E_c - E_{corr}$  in the SO<sub>2</sub>-saturated seawater.

Table A2: Pitting potential  $E_c$ , corrosion potential  $E_{corr}$  and resistance to pitting given in units of  $E_c - E_{corr}$  for 304 SS, 316 SS, and Alloy 825 immersed in SO<sub>2</sub>-saturated seawater at  $T = 80^\circ\text{C}$

Alloy	Test	$E_c$ (mV)	$E_{corr}$ (mV)	$E_c - E_{corr}$ (mV)	Immersion test
304	SS	-268	-80 to -10	-148 to -258	Pitted
316	SS	-60	-140 to -80	20 to -80	Pitted
825	SS	70	-100 to -60	170 to 110	Pitted

Values reported in Table A2 appear in Fig. A3 for 304, 316, and 825 in the SO<sub>2</sub>-saturated seawater case, showing that Alloy 825 has the largest difference  $E_c - E_{corr} = 140$  mV, SCE and therefore the highest pitting resistance (see green bars).



	$E_c$	$E_{corr}$	$E_c - E_{corr}$
Alloy 825	70	-80	140
316 SS	-60	-110	-30
304 SS	-268	-45	-203

Figure A3: Pitting potential  $E_c$ , corrosion potential  $E_{corr}$  and resistance to pitting given in units of  $E_c - E_{corr}$  for 304 SS, 316 SS, and Alloy 825 immersed in SO<sub>2</sub>-saturated seawater at T = 80°C [Scarberry et al, 1979].

### Effect of Mo Content on Pitting

Resistance to pitting corrosion is improved with increasing Mo content in the alloy. Note that 304 SS has no Mo, and both 316L and Alloy 825 have low Mo content (2- 3% Mo and 3% Mo (w/w), respectively). It is important to mention that other alloys with higher Mo content, like Alloys C-276, C-4, C-22, and Alloy 625 (16%, 14 - 17%, 12.5 - 14.5%, 9% w/w, respectively) are discussed in [Gdowski, 1991]. An example of this behavior is given by Asphahani who conducted constant potential tests for 316 SS, Alloy 825, C-276, and Alloy 625 in a 3.8% FeCl<sub>3</sub> solution at 70°C [Asphahani, 1980]. Figure A4 shows that localized corrosion decreases with larger Mo additions.

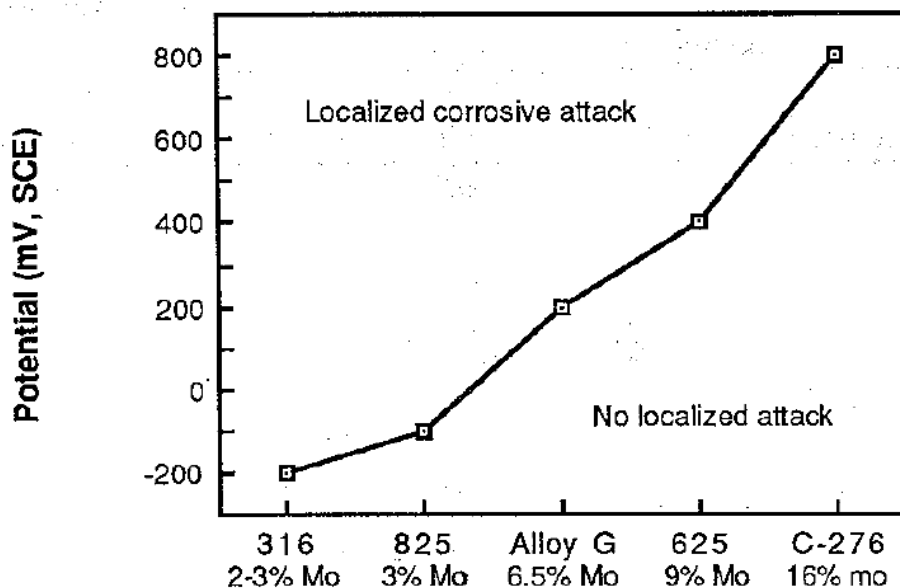


Figure A4: Localized corrosion decreases with larger Mo additions in constant potential tests performed for 316 SS, Alloy 825, C-276, and Alloy 625 in 3.8% FeCl<sub>3</sub> at 70°C [Asphahani, 1980].

### Corrosion resistance of welded austenitic alloys

Welding problems that are specific to the candidate austenitic steels 304L, 316L, and Alloy 825 for HLRW are listed below (Taken from “Overview – Survey of Degradation Modes of Candidate Materials for HLRW Disposal Containers” [Farmer, 1988a]):

#### General Comments on Welding

In the report “Fusion Welding” it is assumed that heating of the surfaces to be joined to  $T > T_m$  and if necessary addition of weld filler metal.

Different zones are defined in a weld. Important to the discussion are FZ and HAZ. FZ corresponds to the fusion zone consisting of filler metal diluted by the surrounding base metal. There is a zone that follows the FZ where a partially melted zone exists. Beyond this region we find the HAZ, where all microstructural changes are restricted to the solid state.

The welding process is intrinsically linked to melting and re-solidification that translates into compositional and microstructural changes of the bulk metal. Examples of compositional changes are: 1) oxygen pick up during the welding and 2) solidification

segregation. Oxygen pick up is reduced using, for example protective inert gas shielding atmospheres. Compositional segregation is responsible for hot cracking. It is generally accepted that the presence of ferrite in the weld metal helps prevent hot cracking.

### **Weld-Induced Sensitization**

Heat affected zones (HAZ) of welds could be affected by  $\text{Cr}_{23}\text{C}_6$  carbide precipitation. All 3 steels, i.e. 304L, 316L and Alloy 825, have chemical compositions that minimize sensitization. Type L steels (304L and 316L) have specific low carbon content ( $\text{C} < 0.03\%$  w/w max.) in their chemical composition and Alloy 825 has Ti which promotes the formation of Ti carbides reducing the loss of Cr.

### **Sigma-Phase Formation and Corrosion of Weld Filler Metal**

Phase stability of the weld metal is also important. The brittle sigma-phase has been found to form during welding of 304L and 316L. Alloy 825 will be stable but welding with Alloy 625, as filler, could lead to a duplex microstructure with coexisting austenite ( $\gamma$ ) and ferrite ( $\alpha$ ).

It is very important to note that the available literature on weld cracking of Alloy 825 is very limited.

More details on the degradation consequences of welded austenitic steels are found in Volume 7: "Weldability of Austenitic Steels" [Strum, 1988]. The author's survey underlines three areas of concern for the welded austenitic steels candidates, i.e.:

- 1) Resistance to corrosion
- 2) Hot cracking
- 3) Formation of intermetallic phases

### **Hot Cracking**

In Volume 7 [Strum, 1988], four stages in hot cracking of stainless steels are mentioned:

- 1) Dendrite formation: solid dispersed in liquid in a continuous way – no crack possible

- 2) Interlocked dendrites: liquid circulating between dendrites – cracks refilled and healed
- 3) Critical solidification range: liquid volumes lack interconnections – cracks cannot be filled
- 4) Liquid completely solidifies – no cracking occurs

Several theories try to explain the reason why ferrite reduces or eliminates hot cracking. Ferrite is believed to act as an impurity sink that prevents GB cracking due to segregation of impurities. The weld metal compositions in both 304L and 316L are adjusted so as to assure a content of ~5% ferrite. This is not possible in Alloy 825 since it is purely austenitic. To prevent hot cracking in Alloy 825, a weld filler of a different composition is used (Alloy 625). The *DeLong* diagram shown in Fig. A5 is an example that shows the work reported in the literature to help design a fusion zone (FZ) in a weld with a given content of ferrite.

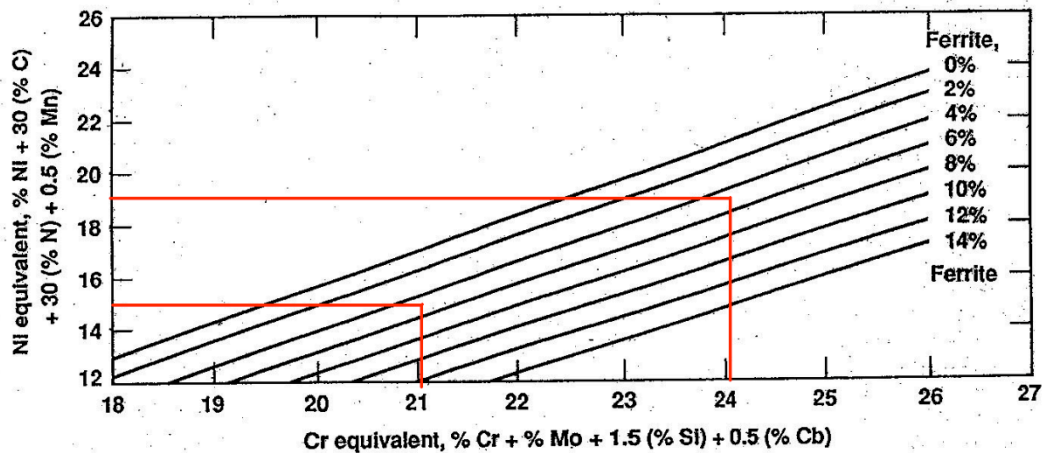


Figure A5: DeLong diagram defines weld chemical composition to obtain different amount of ferrite. Red lines indicate that Cr equivalent values needed to retain 5% ferrite in a typical 316L weld.

Equivalent compositional values are reported in Fig. A5. An example for 316L follows with:

$$\text{Ni equivalent} = \text{Ni} + 30 \text{ C} + 30 \text{ N} + 0.5 \text{ Mn} = 10 + 30 * 0.03 + 0.5 * 2 = 14.9 \sim 15$$

where Cr, Mo, Si, and C<sub>b</sub> (see Fig. A5) are the element chemical composition in wt% (w/w). Red lines in the graph indicate typical Ni equivalent values for 316L equal to 19 and 15, for

316L containing 10% (w/w) or 14% (w/w), respectively and those of the corresponding Cr equivalent needed to obtain a weld that retains 5% ferrite.

It is important to note that a survey [Strum, 1988] on weld cracking of Alloy 825, mentions that Alloy 825 is known to hot crack and adds that no published data is available in the literature on hot cracking effects in Alloy 825. The authors [Strum, 1988] recommend studies to be performed to get a full understanding of hot cracking causes in Alloy 825. They also suggest *friction welding* as a possible means of joining that does not involve melting.

### **Corrosion of welds in austenitic steel candidates**

Sensitization is the most common cause of weld-related intergranular corrosion in austenitic alloys. Sensitization is the precipitation of metal carbides,  $M_{23}C_6$  usually Cr carbides, on the GB which mirrors a depletion of Cr in the region near the GB with a deleterious impact on the materials corrosion resistance. Among the theories that attempt to explain intergranular corrosion of sensitized austenitic steels we should consider the “Cr depletion theory” from [Bain, 1933]. The theory assumes:

- 1) Cr in the bulk material (13 - 15%, w/w) is sufficient to provide a protective passive film
- 2) Cr in the region near to a carbide precipitate has a Cr content lower than that required for passivation.

Precipitation of Cr-rich carbides occurs during sensitization heat treatments.  $M_{23}C_6$  carbide precipitation in welds takes place in the temperature range of 550°C to 800°C. (Note: the M in  $M_{23}C_6$  can be Cr or Fe or Mo).  $M_{23}C_6$  carbides have a tendency to precipitate along GB. Precipitation of  $Cr_{23}C_6$  carbides at GB is at the origin of the Cr-depletion of the surrounding area, to a point that is below the critical level needed for passivation, as shown in Fig. A6, see also Povich. [Povich, 1978]:

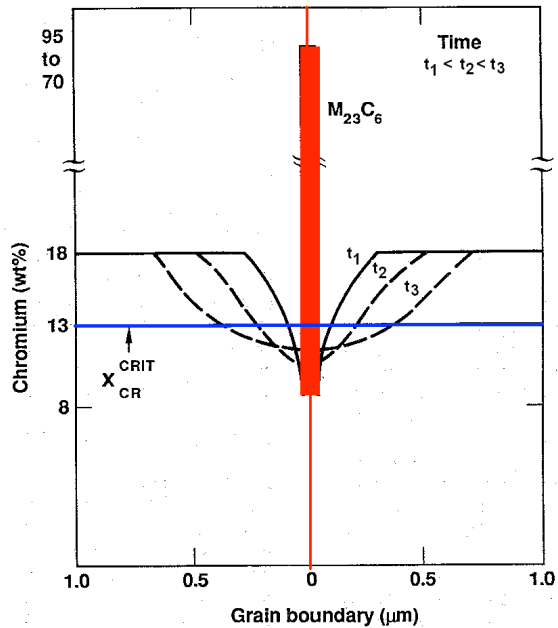


Figure A6: Cr content along the GB region is schematically represented at different times ( $t_1 < t_2 < t_3$ ), underlying the fact that the region depleted in Cr is growing as a function of time. A Cr concentration of ~13% (w/w) is assumed to be the critical Cr concentration needed for passivation to occur (indicated by the blue line).

### Long Storage Times and Low-Temperature Sensitization (LTS)

Low-temperature sensitization was of major interest to the Nevada Nuclear Waste Storage Investigations (NNSWI) Project. Both 304L and 316L are reported to be susceptible of LTS. LTS is a nucleation and growth phenomenon, where carbides nucleate during the sensitization heat treatment and then grow while exposed to temperatures  $T \sim 400^\circ\text{C}$  for long time. Significant increase in GB carbides size in a SS weld is found after 10 days LTS at  $400^\circ\text{C}$ , see Fig. A7 [Povich, 1978].

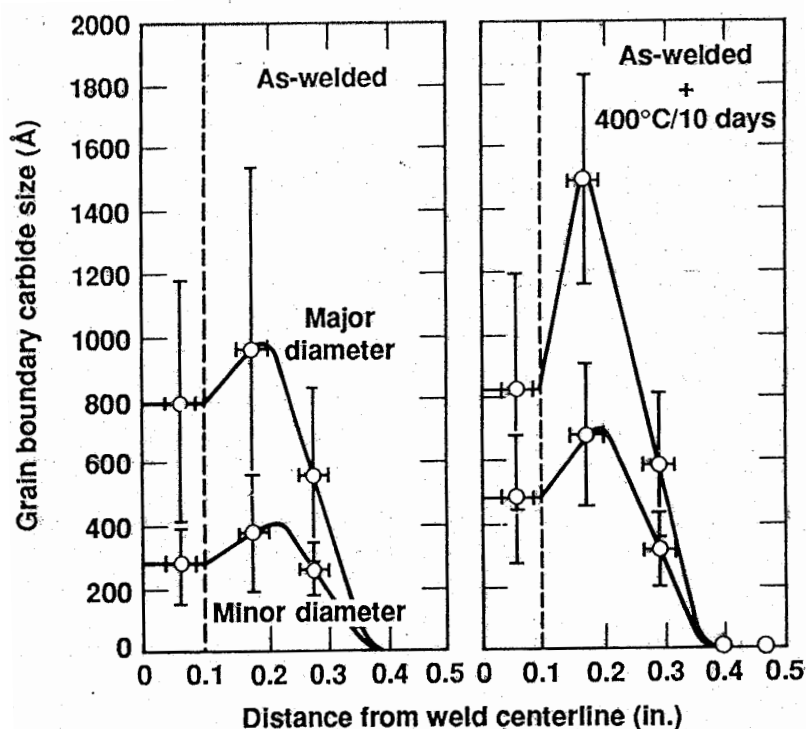


Figure A7: Consequences of Low-temperature sensitization (LTS) on the carbide size; (left) before LTS heat treatment, (right) after LTS heat treatment at 400°C for 10 days.

Difficulties in the evaluation of the consequences of LTS are linked to the short-term exposures and the prediction of long-term growth. Also, the authors underline that there is data on the loss of corrosion resistance due to LTS in 304L SS. No data is available for 316L. Even less information is available on LTS of Alloy 825; it would appear, however, that the high-nickel alloys are not subject to LTS.

### Hydrogen Embrittlement in Austenitic Steels

No consensus is reported in the literature survey [Farmer 1988a, Gdowski, 1988b] on the hydrogen embrittlement (HE) mechanism in austenitic steels. Experiments in the literature survey [Gdowski, 1988b] show that hydrogen embrittlement occurs in the three candidate austenitic steels: 304L, 316L and Alloy 825. It is important to note that there is a [quote] “definite lack of literature” on the effects of hydrogen in Alloy 825.

## Hydrogen Embrittlement Effects

Hydrogen and other corrosive species have been shown to cause sensitized alloys to stress corrode more easily than the unsensitized alloys. Alloys with low carbon content, such as 304L (C = 0.03% w/w max), 316L (C = 0.03% w/w max) and Alloy 825 (C = 0.05% w/w max) have enhanced resistance to sensitization that should be reflected in higher HE resistance. Briant [Briant, 1981] suggests that resistance to HE in austenitic steels is linked to martensitic formation. In 1954, Angel defines the temperature for inducing austenite to martensite transformation,  $M_d$ , in terms of the elemental composition of the alloy given by [Angel, 1954]:

$$M_d (C) = 413 - 462 (C+N) - 9.2 \text{ Si} - 8.1 \text{ Mn} - 13.7 \text{ Cr} - 9.5 \text{ Ni} - 18.5 \text{ Mo}$$

According to this, 316L SS with a low  $M_d$  should be a more stable alloy against martensite transformation, more stable than 304L SS and Alloy 825, and therefore more resistant to HE.

## Degradation of Mechanical Properties Due to Hydrogen Embrittlement

Low concentrations of H (~30 appm) have been shown to degrade primarily the ductility of the material, i.e. the material becomes more brittle; shown in Fig. A8 by a reduction in the elongation [Graver, 1984]. The degradation of elongation is larger in 304 SS (red line) than in 316 SS (blue line) or Alloy 825 (black line). In the experiment, H was cathodically charged for periods of 2 to 32 days.

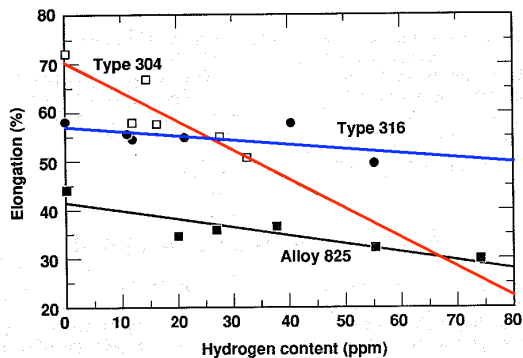


Figure A8: Large reduction in elongation in 304 SS is found at relative low (~30 appm) amounts of hydrogen (red line). 316 SS (blue) and Alloy 825 (black) have a similar dependence, with absolute values always lower for Alloy 825 than for 316 SS.

Yield strength (YS) and tensile strength (UTS) also show degradation as a function of H concentration in both 304 SS and 316 SS as shown in Fig. A9.

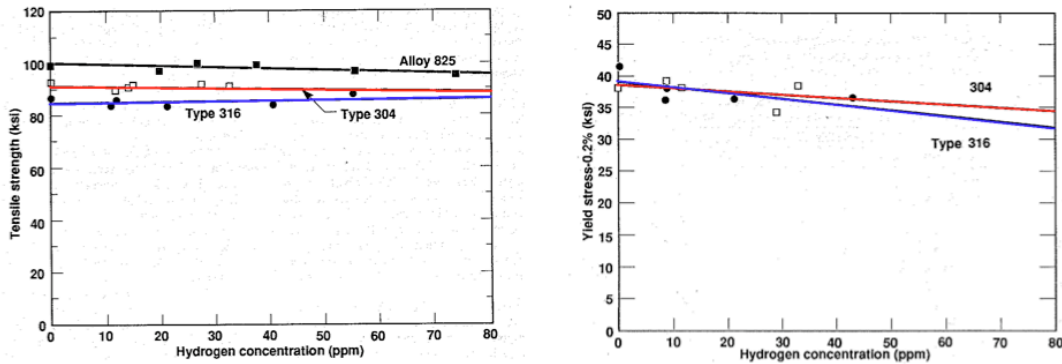


Figure A9: Degradation of mechanical properties induced by hydrogen charging in: a) UTS in 304 SS, 316 SS and Alloy 825 (left) and b) 0.2%YS in 304SS and 316 SS (right).

It has been shown experimentally that 304L steel loss of elongation is recovered after aging at 100°C. This is shown in Fig. A10, where the percent-elongation is reported as a function of aging time.

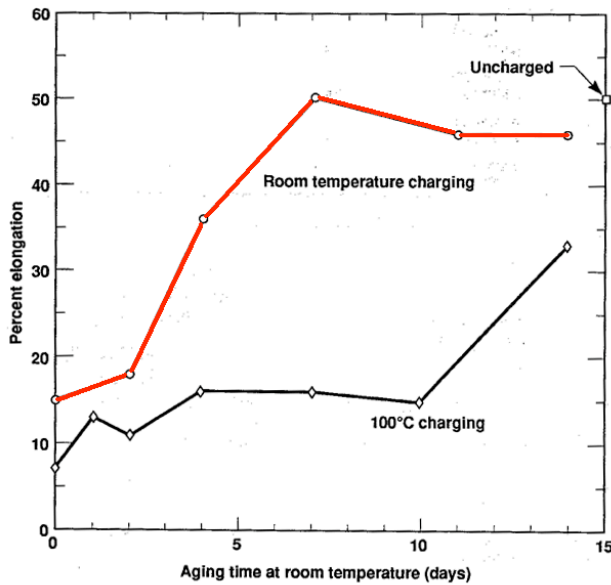


Figure A10: Loss of ductility is recovered after aging at 100°C in both 304L SS specimens, a) specimen charged with H at RT (red line) and b) specimen charged with H at 100°C (black line).

In the experiment shown above [Holzworth, 1969], the steel was first charged at two temperatures (RT and 100°C) and then the percent elongation was measured as a function of aging time (days). The charging with H was performed in a non-hydrogen atmosphere, i.e. charging conditions 1N H<sub>2</sub>SO<sub>2</sub> and 0.1 A/cm<sup>2</sup>. Both specimens show elongation recover after aging for 15 days. A specimen charged at RT shows a faster recovery than a specimen charged at 100°C. A specimen not charged with H shows ~50% elongation after aged for 15 days at 100°C. The specimen charged at RT reaches ~47% elongation after 15 days as compared to ~32% for the specimen charged at 100°C.

It is important to examine hydrogen diffusivity (D) and solubility (S) in these materials. Note that no properties are reported in the degradation mode survey for Alloy 825 diffusivity or solubility - they are assumed to be those of nickel in the discussion. Also, no data for 316 SS diffusivity or solubility was reported. D and S for 316 SS are assumed to be similar to that of 304 SS for which data is available [Perng 1986] that shows low diffusivity and low solubility of hydrogen in this steel. At temperatures relevant to repository environment, D and S are small in magnitude, e.g. at T = 25°C. Hydrogen diffusivity in 304 SS is  $D = 4 \times 10^{-12}$  cm<sup>2</sup>/s, while at T = 275°C diffusivity reaches  $D = 7 \times 10^{-8}$  cm<sup>2</sup>/s. Both diffusivity and solubility in 304 SS increase as temperature increases (Arrhenius behavior). Hydrogen solubility in 304 SS is ~100 - 300 appm for the same temperature range.

## **Phase Stability**

Alloy 825 (*Incoloy*) is an austenitic Ni-Fe-Cr alloy with additions of Mo, Cu, and Ti. Alloy 825 phase stability is better than that of 304L and 316L SS [Bullen, 1988]. Figure A11 shows that 304L and 316L SS are closer to the  $\alpha+\gamma$  phase region while Alloy 825 is well within the  $\gamma$ -phase.

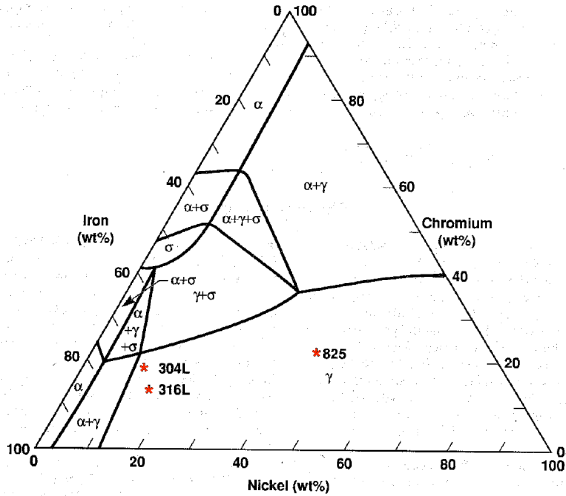


Figure A11: Fe-Cr-Ni equilibrium phase diagram at 650°C. Note: stars help locate 304L, 316L and Alloy 825.

Martensitic transformations have not been observed in Alloy 825. Martensitic transformations occur in 304L and 316L SS. Also, the sigma-phase has been observed in 316L promoted by the presence of Si. The formation of a sigma-phase can result in significant degradation of the 316L mechanical properties. Also, GB attack could result from the  $M_{23}C_6$  carbide precipitation in both 316L and 304L SS.

A heat treatment is proposed that enhances Alloy 825 resistance to sensitization. Sensitization involves the precipitation of Cr-rich  $M_{23}C_6$  carbides at the GB that in turn causes a depletion of Cr in the adjacent region. Since Cr is responsible for the corrosion resistance of these alloys via the formation of thin uniform Cr-oxide layers on the surface, the loss of Cr in the matrix translates into localized intergranular attack that can occur when the material is exposed to corrosive service conditions. A stabilization heat treatment (annealing at 970°C to 925°C for 1 hr) enhances Alloy 825's resistance to sensitization. Alloy 825 contains Ti, which is a strong 'getter' of carbon. Ti removes the carbon from solution and prevents alloy additions (such as Cr) from forming carbides. The heat treatment is specified to ensure that Ti has consumed the carbon.

Among the copper alloys, CDA 102 (OFHC Cu) is ranked as the one with the best phase stability followed by CDA 715 and CDA 613. CDA 102 is a single-phase material (CDA 102 is essentially pure Cu). CDA 715 (Cu with 30% Ni, w/w) and CDA 613 (Cu with 6.8% Al, w/w) are solution-hardened materials that offer improved mechanical and corrosion

performance. The review study performed in 1988 [Farmer, 1988a] shows that these materials would remain single-phased to at least 300°C, see the case of CDA 613 in Fig. A12.

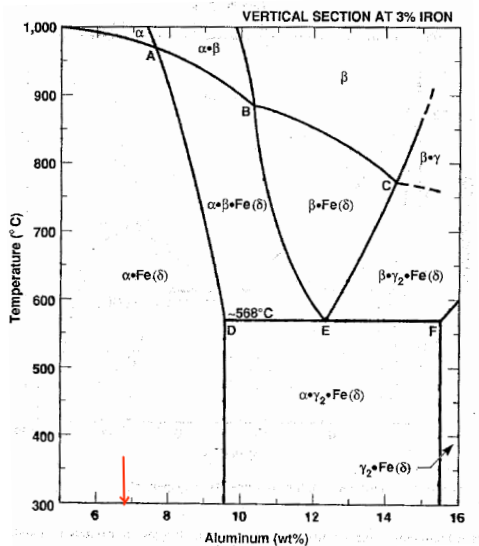


Figure A12: Cu-Al-3%Fe phase diagram showing that CDA 613 with a composition of Cu (6.8% Al, w/w) is single-phased ( $\alpha$ -phase) with iron precipitates [Fe( $\delta$ )].

Migration and precipitation of Fe in CDA 715 and CDA 613 and of Sn in CDA 613 may cause material degradation. Precipitates of Fe in CDA 613 may grow in size over extended periods of time. Also, it is believed that Fe<sub>3</sub>Al is formed in CDA 613, which would mean that Fe diffusion would be less than that of free Fe in Cu.

### Phase stability in Ni-Cr-Mo alloys

Using Calphad methodology, property diagrams were calculated for several Ni-Cr-Mo based alloys at their nominal alloy compositions [Turchi, 2006]. These diagrams display the phase fraction of each stable phase as a function of temperature. These alloys (at equilibrium at low temperature) exhibit part of the fcc matrix, long-range order (LRO) of Pt<sub>2</sub>Mo-type indicated by the formation of oP6 phase, complex Frank-Kasper phases (P and  $\sigma$  phases), carbides and silicides at low phase fraction. Figure A13 shows this happening in C-4 and C-276 Alloys and Fig. A15 below shows similar findings in C-22. (Note that the authors also show that W has a positive effect of destabilizing the oP6 phase).

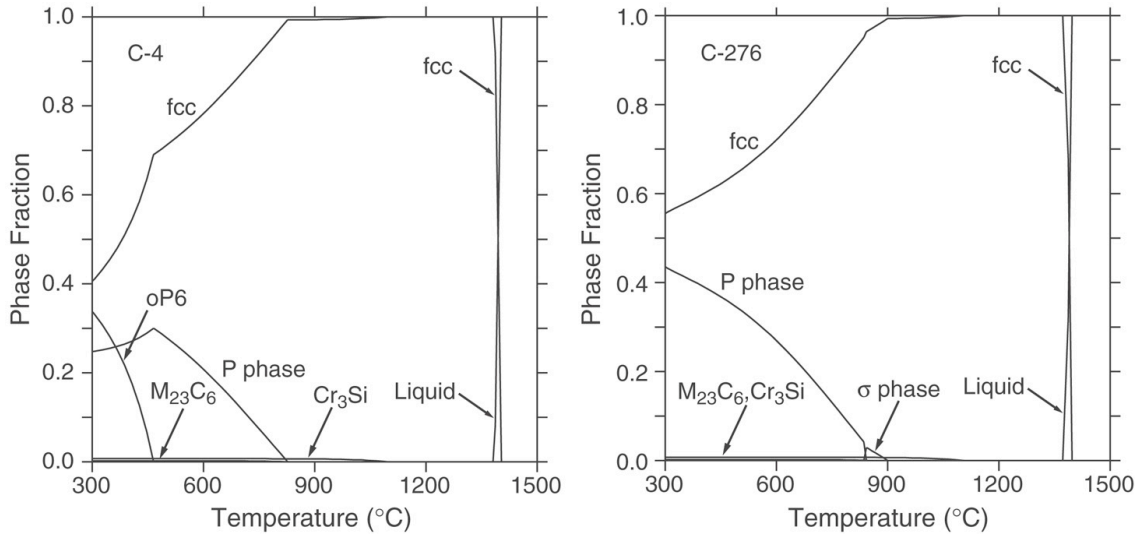


Figure A13: Phase fraction diagram for a) C-4 (left) and C-276 alloys (right) indicating that at equilibrium and at low temperatures oP6 LRO phase, P and sigma phases are present.

#### C-4

In the case of Alloy C-4, Turchi [Turchi, 2006] shows that the main phases forming, besides the fcc matrix, are the P- and oP6-phases, and at very low phase fraction the M<sub>23</sub>C<sub>6</sub> and the A15 Cr<sub>3</sub>Si-type phases; see Fig. A13a (left). The relatively low content in Cr in this alloy excludes the formation of the  $\sigma$ -phase.

#### C-276

In the case of Alloy C-276, as in the case of alloy C-4, Turchi [Turchi, 2006] shows that the low content in Cr and Mo significantly reduces the formation of the  $\sigma$ -phase and prevents the formation of the oP6-phase; see Fig. A13b (right). Because of the presence of C and Si, the A15 of Cr<sub>3</sub>Si-type and M<sub>23</sub>C<sub>6</sub> are found in this alloy as in the C-4 alloy.

#### Alloy C-22

Turchi [Turchi, 2006] discusses a comparison of predicted results and experimental findings for Alloy 22.

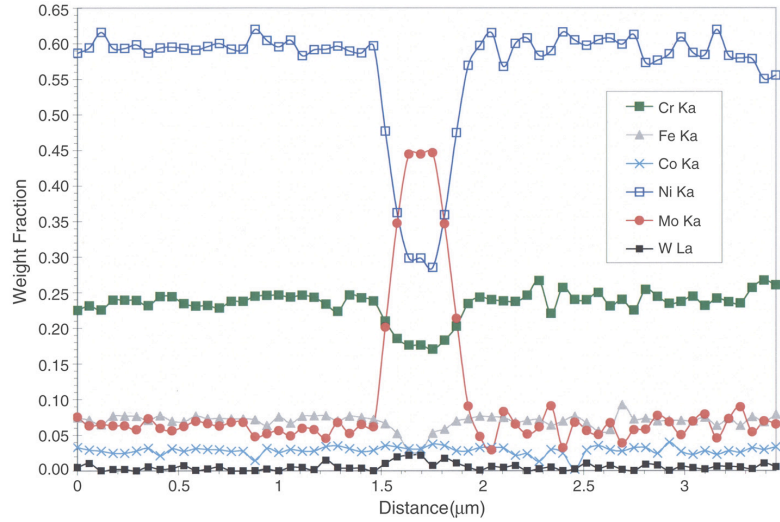


Figure A14: Platelet of P-phase precipitate in Alloy 22 annealed for 22 h at 704°C a) Micrograph (left) and b) EDX Experiment (right) [Shen, 2000].

The authors report a micrograph (see Fig. A14a, left) that shows a platelet of P-phase precipitate in a fcc matrix of Alloy C-22 annealed at 704°C for 22 hours [Shen, 2000]. EDX spectroscopy experiment across the red straight line in the micrograph shows a decrease in Ni content in the platelet (open blue squares in the weight fraction vs. distance plot in Fig. A14b, right), increase in Mo content (red circles) in the platelet. Also they report some evidence of decrease in Cr (green line) and Fe (open triangles) and a slight increase in W (small black solid squares at the bottom of the plot). There is no evidence of solute depletion in the zone surrounding the platelet.

Property diagrams derived for Alloy 22 using *Calphad* methodology are shown in Fig. A15. The diagram on the left corresponds to phase fraction as a function of temperature; with the straight line in the figures indicating the annealing temperature in the experiment, i.e. T = 704°C. The diagram shows that at this temperature P-phase forms in the alloy with a phase fraction of ~20%.

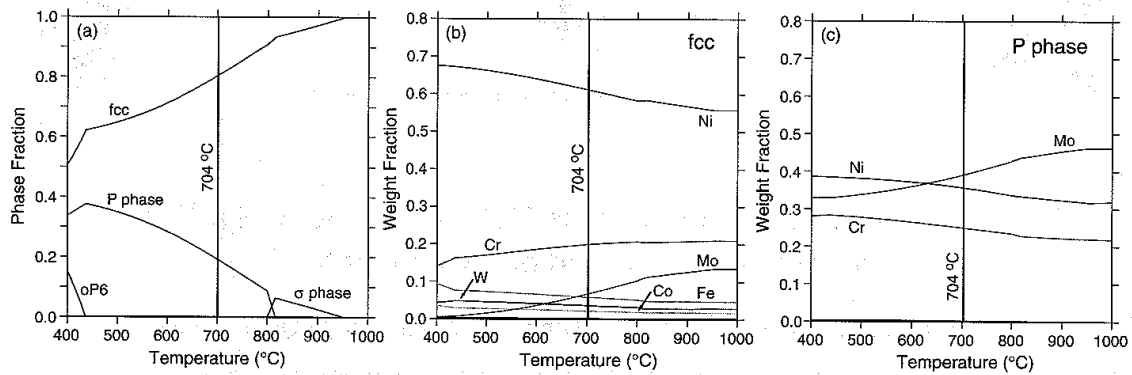


Figure A15: Phase fraction diagram for Alloy 22 as a function of temperature (left). Weight fractions of elements in Alloy 22 as a function of temperature a) in fcc phase (center) and b) in P phase (right).

Also shown in Figure A15 are the weight fractions for Alloy 22 in fcc phase (center) and in P phase (right). These diagrams indicate that in the fcc phase at  $T = 704^{\circ}\text{C}$ , the composition of the alloy is that of the starting fcc condition while in the P phase, there is a larger weight fraction of Mo than Ni and Cr indicating a fair agreement with the experimental evidence.

### Kinetics of Phase Transformations in Ni-Cr-Mo Alloys

The ordering transformation that takes place in these Ni-Cr-Mo based alloys has been linked to an increased susceptibility to SCC and hydrogen embrittlement. In 2007, the kinetics of phase transformations in Ni-Cr-Mo alloys was investigated [Turchi, 2007] aimed at predicting the rate at which LRO is occurring in Alloy 22 under repository conditions. The authors conclude that the diffusion kinetics in the temperature range where the formation of the LRO phase of  $\text{Ni}_2\text{Cr}$ -type occurs is extremely slow. It is therefore very unlikely that the ordered phase will form under repository conditions, i.e., below  $200^{\circ}\text{C}$ , even for as long as 100,000 years.

Using the *Calphad/Dictra* methodology, the authors determine the kinetics of transformation in Alloy 22 from a fcc matrix to the oP6-ordered phase, fcc to P, and fcc to  $\sigma$ -phase, see Fig. A16. The temperature-time transformation (TTT) diagram shows the critical

order-disorder temperature is 596°C (left), the transformation temperature is about 836°C and 727°C for P- and  $\sigma$ -phase, respectively.

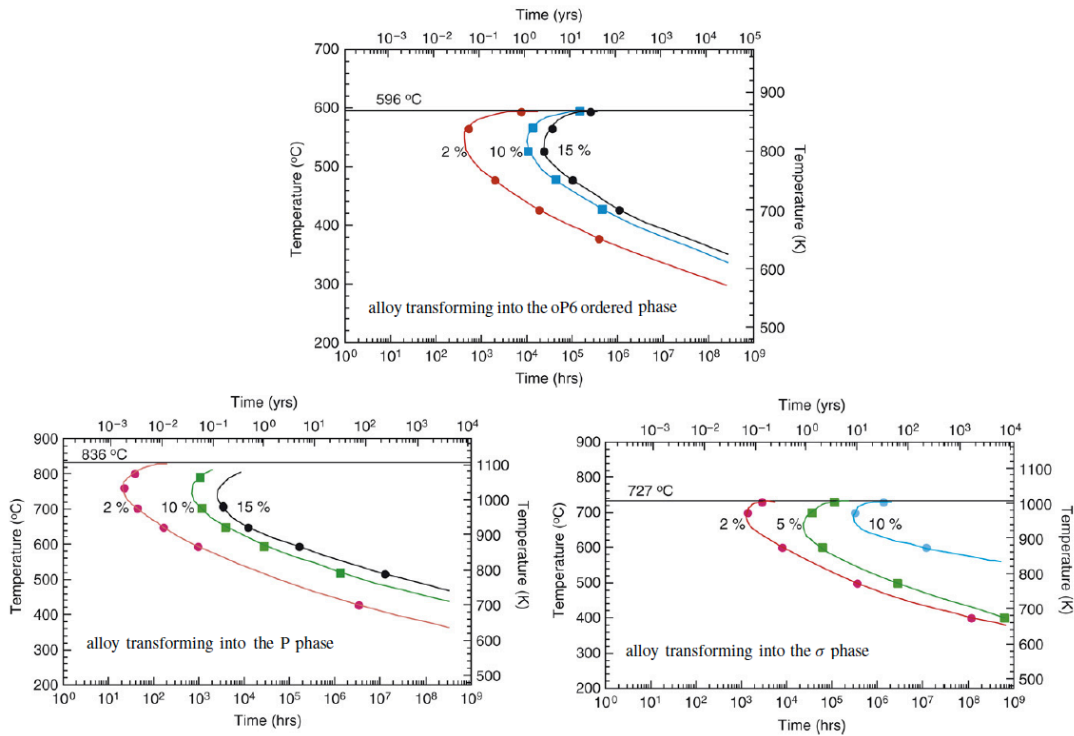


Figure A16: Kinetics of transformations from fcc to oP6-phase (top) and from fcc to P (bottom left) and from fcc to  $\sigma$ -phase (bottom right) in Alloy 22.

Simulation results and volume-fraction measurements [Torres, 2003] are shown in Fig. A17 at two temperatures  $T = 700^{\circ}\text{C}$  and  $T = 750^{\circ}\text{C}$ . Simulations and measurements show agreement and indicate that the phase transformation occurs in reality at a slower pace than predicted.

Also, experimental findings from [Karmazin, 1994] indicated in Fig. A18 by blue squares and results predicted with *Dictra* for a Ni-Cr binary alloy (blue circles corresponding to the label 10%  $\text{Ni}_2\text{Cr}$ ) are shown together with isothermal TTT diagrams for Alloy 22 transformation in P-phase (black lines) and qualitative observations performed at LLNL [Torres, 2003], see labels on GB coverage, LRO and bulk precipitation. Again good compatibility was found between experiments and predictions.

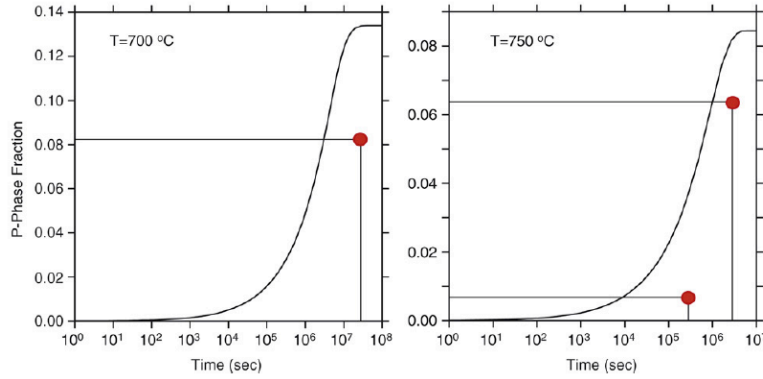


Figure A17: Volume fraction measurements of fcc to P transformation in Alloys 22 [Torres 2003] as compared to predicted results [Turchi, 2007]

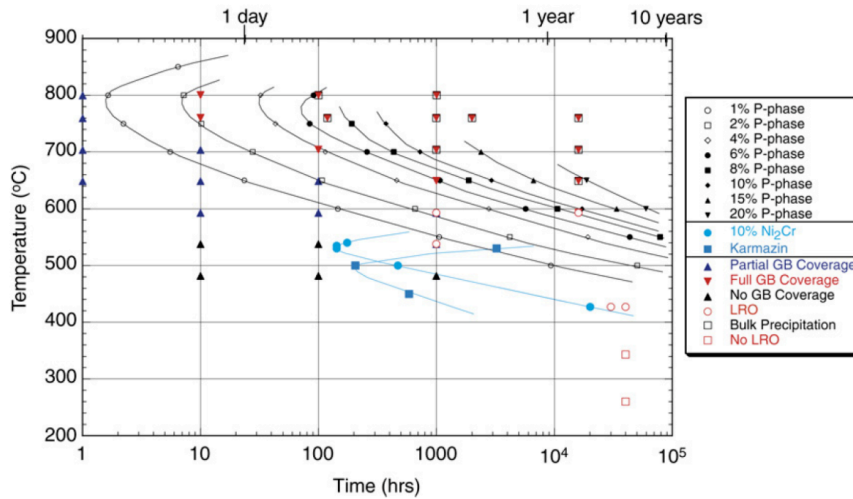


Figure A18: Isothermal TTT diagram a) calculated for a binary Ni-Cr alloy with a 10% transformation of the fcc matrix in the oP6-ordered phase of Ni<sub>2</sub>Cr-type; see lower curves describing the prediction (blue circles) and the results extracted from the experimental work of Karmazin (blue squares) [Karmazin, 1994] and b) calculated for a fcc-based matrix of a surrogate of Alloy 22 transforming into the P-phase (black lines), with transformation from 1% (open circles) to 20% (down triangles).

## References

- [Angel, 1954]** T. Angel, "Formation of Martensite in Austenitic Stainless Steels: Effects of Deformation, Temperature, and Composition", J. of the Iron and Steel Institute 177 (1954) 165.
- [Asphahani, 1975]** A. I. Asphahani, H. H Uhlig, "Stress Corrosion Cracking of 4140 High Strength Steel in Aqueous Solutions", Journal of the Electrochemical Society 122,2 (1975) 174.
- [Asphahani, 1980]** A. I. Asphahani, "Localized Corrosion of High Performance Alloys", Materials Performance 19, 8 (August 1980) 9-21.
- [Bain, 1933]** E. C. Bain, R. H. Abron, J. J. B. Rutherford, "The Nature and Prevention of Intergranular Corrosion in Austenitic Stainless Steels", Trans. Amer. Soc. for Steel Treating 21 (1933) 481.
- [Briant, 1981]** C. L. Briant, "Hydrogen assisted cracking of austenitic SS", Hydrogen Effects in Metals, Eds. I. M. Bernstein, A. W. Thompson, The Metallurgical Society AIME (1981) 527.
- [Bullen, 1988]** D. B. Bullen, G. E. Gdowski, "Phase Stability – Vol. 1", UCID-21362 Vol. 1, August 1988.
- [Copson, 1959]** H. R. Copson, Physical Metallurgy of Stress Corrosion Fracture, Interscience, 1959, 247.
- [Farmer, 1988a]** J. C. Farmer, R. D. McCright, J. N. Kass "Survey of Degradation Modes of candidate Materials for High-Level Radioactive-Waste Disposal Containers- Vol. 3 Overview", UCID-21362 Overview, June 1988.
- [Farmer, 1988b]** J. C. Farmer, R. A. Van Konynenburg, R. D. McCright, D. B. Bullen "Survey of Degradation Modes of candidate Materials for High-Level Radioactive-Waste Disposal Containers- Vol. 3 Localized Corrosion and Stress Corrosion Cracking of Austenitic Alloys", UCID-21362 Vol. 3, April 1988.
- [Furuya, 1985]** T. Furuya, T. Fukuzuka, K. Fujiwara, H. Tomari, "Gamma-Ray Irradiation Effects on Stress Corrosion Cracking of Alloys for a High

- Level Liquid Waste Package”, R-D Kobe Sielosho Gijutsu Hokoku, Vol. 33, No.1 , January 1983, PP. 43-46.
- [Gdowski, 1988a]** G. E. Gdowski, D. B. Bullen, “Oxidation and Corrosion – Vol.2”, UCID-21362 Vol. 2, 1988.
- [Gdowski, 1988b]** G. E. Gdowski, D. B. Bullen, "Effects of Hydrogen in Austenitic and Copper-Based Alloys – Vol. 6", UCID-21362 Vol. 2, August 1988.
- [Gdowski, 1991]** G. E. Gdowski, “Survey of Degradation Modes of Four Nickel-Chromium-Molybdenum Alloys”, UCRL-ID-108330, March 1991.
- [Graver, 1984]** D. L. Graver, "Hydrogen Permeation and Embrittlement of Some Nickel Alloys", Corrosion of Nickel-Based Alloys, American Society for Metals, Metals Park, Ohio, 1984, 79-85.
- [Holzworth, 1969]** M. L. Holzworth, "Hydrogen Embrittlement of Type 304L SS", Corrosion 25, No. 3 (1969) 107.
- [Karmazin, 1994]** L. Karmazin, J. Krejčí, J. Zeman, “Gamma-Phase and Ni<sub>2</sub>Cr-Type Long-Range Order in Ni-Rich Ni-Cr-Mo Alloys”, Mater. Sci. Eng. A183 (1994) 103-109.
- [Perng, 1986]** T. P. Perng, C. J. Altstetter, “Effects of Deformation on Hydrogen Permeation in Austenitic Stainless Steels”, Acta Met. 34 (1986) 1771.
- [Pope, 1987]** D. H. Pope, “Microbiologically influenced corrosion in the nuclear power industry: Case histories, Methods of detection, control and prevention”, Proceedings of the 3rd Int. Symp. On Environmental Degradation of Materials in Nuclear Power Systems – Water Reactors, Traverse City, Michigan, August 30 to September 1987, The Metallurgical Society, 1988.
- [Povich, 1978]** M. J. Povich, “Low Temperature Sensitization of Type 304 SS”, Corrosion 34, No.2, (1978) 60.
- [Scarberry, 1979]** R. C. Scarberry, E. L. Hibner, J. R. Crum, “Assessment of Pitting-Potential Measurements in Severely Corrosive Environments”, Paper Number 245, Corrosion 79, Atlanta, Georgia, March 12-16, 1979, National Association of Corrosion Engineers, Katy, Texas.

- [Shen, 2000]** T. H. Shen, "X-ray Microanalysis of Precipitates in Alloy C-22", LLNL Technical Memorandum, March 20, 2000 (unpublished).
- [Strum, 1988]** M. J. Strum, H. Weiss, J. C. Farmer, D. B. Bullen "Survey of Degradation Modes of candidate Materials for High-Level Radioactive-Waste Disposal Containers- Vol. 7 Weldability of Austenitic Alloys", UCID-21362 Vol. 7, June 1988.
- [Torres, 2003]** S. Torres. LLNL private communication (April 2003).
- [Turchi, 2006]** P. E. A. Turchi, L. Kaufman, Z-K Liu, "Modeling of Ni-Cr-Mo Based Alloys: Part I - Phase Stability", Computer Coupling of Phase Diagrams and Thermochemistry 30 (2006) 70.
- [Turchi, 2007]** P. E. A. Turchi, L. Kaufman, Z-K Liu, "Modeling of Ni-Cr-Mo Based Alloys: Part II - Kinetics", Computer Coupling of Phase Diagrams and Thermochemistry 31 (2007) 237.
- [Weiner, 1961]** L. C. Weiner, "Kinetics and Mechanism of Hydrogen Attack of Steel", Corrosion 17, No.3 (1961) 137.

## **Appendix B**

### **Waste Package Design Criteria and Waste Environment at Yucca Mountain**

When the degradation mode surveys were written in the late 1980's, a HLRW container was required to maintain mechanical integrity for ~50 years after emplacement to allow retrieval in the pre-closure phase of repository operation. Waste packages were required to provide complete containment for a period of ~300 to 1,000 years. However, with the evolution of 10CFR60 [1] to 10CFR 63 [2], specific requirements for barriers, including waste package post-closure performance, were replaced with requirements for a combination of natural and engineered barriers, and with overall performance of the repository being subject to quantitative requirements. As part of repository development, DOE designed the waste packages for extremely long term performance, hundreds of thousands of years in the repository environment.

After a few years in the repository, containers will face  $T_{\max} \sim 250^{\circ}\text{C}$ , and high  $\gamma$ -radiation. Such  $\gamma$ -radiation will promote radiolytic decomposition of the moist air near the container surfaces. Hydrogen has the potential to alter the metallurgical behavior of the container material. (Note: After ~100 years, the temperature of the container decays to ~150°C).

[1] DOE 10 CFR Part 60: Disposal of High-Level Radioactive Wastes in Geologic Repositories.

[2] DOE 10 CFR Part 63: Disposal of High-Level Radioactive Wastes in Geologic Repositories at Yucca Mountain, NV.

## Appendix C

### **Mechanical Properties of Several Austenitic Steels at Room Temperature**

*Table C1: Mechanical properties of the candidate austenitic alloys at room temperature [1,2]*

<b>Material</b>	<b>UTS [MPa]</b>	<b>0.2%YS [MPa]</b>	<b>Elongation [%]</b>
304 SS	655	241	65
316 SS	586	255	65
Alloy 825	693	301	43

**[1]** Metals Handbook, Volume 2, Properties and Selection: Nonferrous Alloys and Pure Metals, 9th ed. American Society for Metals, Metals Park, Ohio, 1979, 237.

**[2]** Source Book on Industrial Alloy and Engineering Data, American Society for Metals, Metals Park, Ohio 1978, 185-207, 219-223.